

Passive & Active Control of Regenerative Standing & Soliton Waves

(Invited Paper)

William F. Address, David S. Ricketts, Xiaofeng Li, and Donhee Ham
Harvard University, Cambridge, MA 02138

Abstract— This paper reviews two technologies that govern the character of electromagnetic waves, or wave-control technologies, that we recently developed [1,2] in the context of wave-based oscillators. In [1], the component fields of a standing wave hosted by a transmission line are sculpted to better suit the unique standing wave properties; this *passive* wave control is achieved by tapering the transmission line along its length and serves to reduce the oscillator phase noise. In [2] we constructed an oscillator that self-generates a stable, periodic train of electrical solitons. In this work, an *active* amplifier controls the “unruly” soliton dynamics to guarantee oscillation stability.

Keywords— standing waves, solitons, oscillators, (nonlinear) transmission lines, modelocking, pulse generation.

I. INTRODUCTION

WHILE a prevalent class of modern RF & microwave oscillators relies on lumped LC tanks, oscillators that operate instead upon wave behaviors are not uncommon. In the pre-transistor era, GHz signal generation was done predominantly by oscillators consisting of electron beams coupled with waveguides or cavities [3]. These electron-beam oscillators were indeed wave-based: the backward-wave and klystron oscillators, two prime examples of the oscillator type, operate using travelling and standing waves, respectively.

The advent of the transistor and microfabrication technology in later years gradually ushered in the time for solid-state wave-based oscillators, often in an integrated form. Transistors combined with a planar waveguide (transmission line) yield travelling wave oscillators (recent examples: [4] - [7]) while transistors coupled with a planar cavity (transmission line with reflective or periodic boundaries) lead to standing wave oscillators (recent works: [8,9]).¹

The wave-based oscillators strongly fulfill certain design criteria. For example, the wave on the transmission line readily lends itself to distributed amplification by transistors spread along the line, facilitating high-frequency oscillations [4] - [6]. In another example, wave-based oscillators were ingeniously used for low-skew/jitter clock distribution [7,8]. In suitable applications, therefore, wave-based oscillators could one day become an indispensable feature.

Working in this area of wave-based oscillators, the authors recently advanced two new technologies, *Standing-wave adaptive line tapering* and the *electrical soliton oscillator*, whose review is the purpose of this article.

Standing-wave adaptive line tapering: Previously the advantages of wave behaviors in terms of resonator Q and oscillator phase noise were not readily apparent. In [1], we addressed this issue, presenting a case where ex-

ploitation of wave behaviors proves beneficial in enhancing Q and lowering phase noise. Standing waves have the unique property of position-dependent voltage-current amplitudes. We demonstrated that the loss characteristics of a transmission line hosting standing waves can be adapted to these amplitude variations through a position-dependent structuring (*tapering*) of the line to reduce loss, leading to Q improvement and phase noise reduction (up to 10 dB).

Electrical soliton oscillator: This work marks a distinctive departure from the conventional sinusoidal wave-based oscillators: reporting in [2], we introduced the electrical circuit that self-generates a periodic, stable train of unique nonlinear pulses known as electrical solitons. Solitons are unique pulse-shape waves that exhibit singular nonlinear behaviors as they propagate in nonlinear media. Solitons *per se* are well known phenomena that have captivated scientists over a century. In the electrical domain, the nonlinear transmission line (NLTL) [1D lattice of inductors and varactors: Fig. 1(a)] has been extensively used to create electrical solitons over the past 40 years for sharp pulse generation [10]. In these developments, however, the NLTL has been almost exclusively used as a “2-port (input + output)” system that requires an external high-frequency input to produce the soliton output [Fig. 1(a)]. What distinguishes our circuit in [2] is that it is an oscillator [“1-port (output only)” system] that self-generates electrical solitons without requiring an external high-frequency input. Our soliton oscillator was made possible by connecting the NLTL around a unique amplifier [Fig. 1(b)]. By nature, electrical solitons are “unruly,” which had rendered previous attempts to build the soliton oscillator unsuccessful, usually resulting in chaotic oscillations [11]. The key to our success was finding a way to “tame” the solitons: the amplifier was uniquely engineered to stabilize soliton oscillation, in addition to providing gain. The electrical soliton oscillator now mirrors the already-mature soliton lasers in optical modelocking.

“The common thread”: Our two technologies above share in their essence a common feature: *wave control*. The tapering of the passive transmission line is to control the wave’s field distribution on the line: this passive control exploits the unique standing wave properties for improving phase noise. In the electrical soliton oscillator, the active amplifier controls the “unruly behaviors” of soliton waves: this active control suppresses soliton’s inherent instability-prone dynamics to guarantee oscillation stability. This paper is a review of these two technologies: Secs. II and III review the wave-adaptive line tapering and the electrical soliton oscillator, respectively. Detailed descriptions can be found in [1] and [2], and related articles in [12] and [13].

¹Dielectric oscillators are another solid-state example.

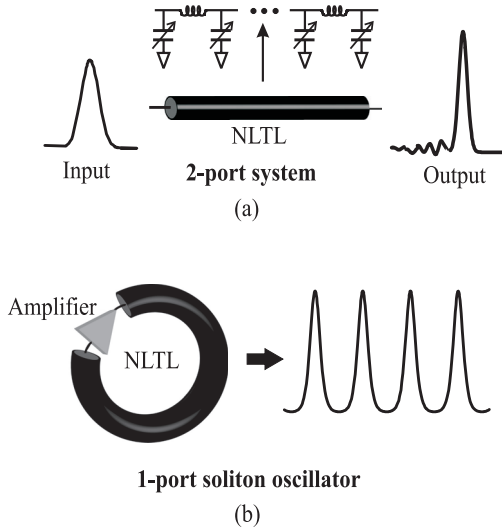


Fig. 1. (a) 2-port NLTL. (b) 1-port soliton oscillator.

II. STANDING-WAVE ADAPTIVE LINE TAPERING

This section reviews our work on standing-wave adaptive transmission line tapering for lowering phase noise of standing wave oscillators [1]. The quarter-wavelength ($\lambda/4$) standing wave oscillator (SWO) of Fig. 2(a) will be used as a demonstrational vehicle. In this most compact SWO configuration, a differential transmission line is connected to a pair of cross-coupled inverters at one end and is shorted at the other end. The cross-coupled inverters may be realized using cross-coupled transistors [Fig. 2(b)].

In the SWO of Fig. 2(a), energy injected by the cross-coupled inverters propagates in forward waves along the line toward the short, where the energy is reflected into reverse waves. In steady state, the forward and reverse waves superpose to form standing waves. In the fundamental mode ($l = \lambda/4$), voltage amplitude, $V(z)$, and current amplitude, $I(z)$, exhibit monotonic variations with z as depicted in Fig. 2(a). The voltage minimum (zero) and current maximum occur at the short end ($z = l$) while the voltage maximum and current minimum occur at $z = 0$. Due to transistor loading, the amplitude of this current minimum at $z = 0$ is slightly larger than zero, as l is slightly smaller than $\lambda/4$. This amplitude variation in standing waves is the key property that makes possible the transmission line tapering to lower SWO phase noise, review of which will be the subject of the following subsections.

A. Wave Adaptive Line Tapering - Concepts

For silicon integration, the differential transmission line of Fig. 2(a) can be implemented as an on-chip coplanar stripline (CPS) [Fig. 2(c)], composed of two metals running in parallel. Figure 2(c) also shows the familiar differential $LRCG$ model for the on-chip CPS where L , C , R , and G are inductance, capacitance, series resistance, and shunt conductance per unit length, respectively. R mainly accounts for loss within metals due to skin and proximity effects while G reflects loss outside metals (*e.g.*, substrate loss). R couples to current waves as G couples to voltage waves to introduce respective series and shunt losses, di-

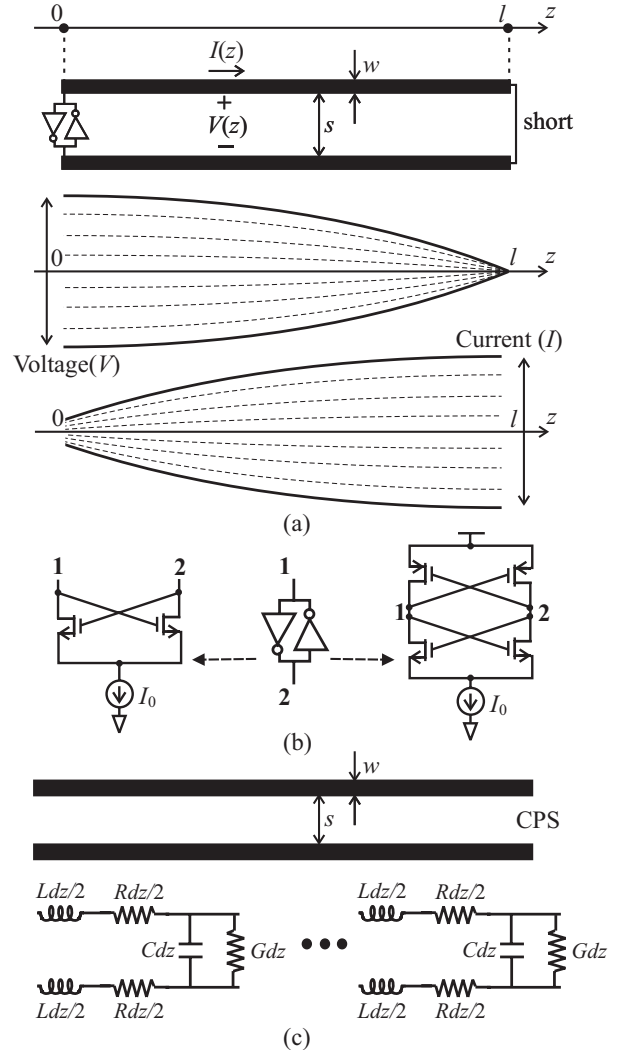


Fig. 2. (a) $\lambda/4$ SWO and standing waveforms at the fundamental mode. (b) MOSFET implementations of the cross-coupled inverters. (c) Coplanar stripline and differential $LRCG$ model.

rectly affecting CPS quality factor, Q , and oscillator phase noise. Low values of R and G correspond to high Q .

Varying metal width, w , and separation, s , of the CPS [w and s are with reference to Fig. 2(c)] is a means of modifying R and G . However, desired simultaneous minimization of R and G is often impossible: increasing w and s decreases R by mitigating the skin and proximity effects, respectively, but increases G by allowing more interaction with the lossy substrate and underlying metals. This tradeoff between R and G imposes a major constraint in overall loss minimization when the CPS carries a traveling wave.

Our key idea in [1] is that when the CPS hosts a standing wave, the R - G tradeoff can be elegantly circumvented to minimize loss, thanks to the position-dependent standing wave amplitudes. As shown in Fig. 2(a), the $\lambda/4$ SWO has a voltage maximum and current minimum near $z = 0$ and vice versa near $z = l$, so power loss is dominated by shunt conductance G toward $z = 0$ and by series resistance R toward $z = l$. Therefore, G may be minimized to reduce loss near $z = 0$ while the unavoidable increase in R (due to the R - G tradeoff) is not detrimental because of

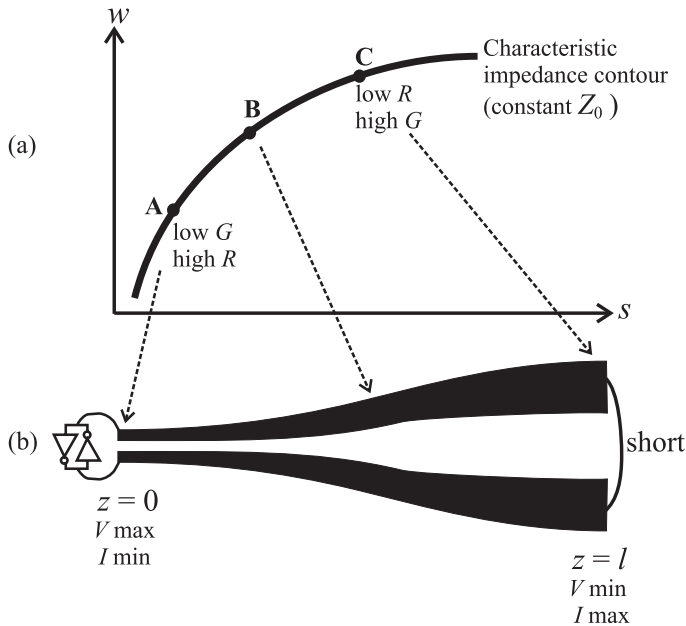


Fig. 3. (a) Simulation-based characteristic impedance contour and R - G variations in w - s space. (b) $\lambda/4$ SWO using a tapered CPS.

the negligible current amplitude in this vicinity. Similarly toward $z = l$, R may be minimized to reduce loss while the inevitable increase in G is innocuous due to the locally negligible voltage amplitude. This continuous variation of R and G along z adapted to the standing wave amplitudes to minimize loss yields a *tapered* CPS structure. Note that the position dependence of the standing wave amplitudes is what makes possible this tapering technique.

In order to prevent local reflections, the transmission line tapering should be performed with attention to holding the characteristic impedance, Z_0 , constant throughout the line. This task is facilitated by comprehensive EM simulation data for various uniform CPSs, which reveal the dependence of R , G , and Z_0 on a wide range of w and s values [1]. Figure 3 shows an example simulation-based contour of constant characteristic impedance in w - s space in a standard CMOS technology. As one simultaneously moves apart (increasing s) and widens (increasing w) the CPS following this contour, Z_0 remains constant while R decreases and G increases. This R - G dependence on w and s is the previously discussed R - G tradeoff. The CPS of the $\lambda/4$ SWO can be tapered along this contour as shown in Fig. 3. The voltage maximum and current minimum at $z = 0$ yields minimum local loss with low G despite high R [point A in Fig. 3(a)]. The current maximum and voltage minimum at $z = l$ yields minimum local loss with low R despite high G (point C). Outside the range from A to C, the R - G tradeoff deteriorates and it becomes difficult to improve either loss. Therefore, no point outside the range is optimal for any position along the standing wave.

Note that while line tapering has been used in the past, traditional line tapering has been solely focused on variation of characteristic impedance with position [1] for applications such as impedance transformation. The novelty of our line tapering lies in producing variations of the loss parameters with position to reduce line loss while keeping

characteristic impedance uniform throughout the line.

B. Wave Adaptive Line Tapering - Theory

This subsection presents an analysis that quantifies the loss reduction and Q improvement owing to the tapering. This analysis was originally conducted in [1].

The total time-averaged loss, P_{diss} , in a general tapered (position-dependent) transmission line with constant characteristic impedance Z_0 , when hosting a single standing wave mode, is given by

$$P_{diss} = \int_0^l \left[\frac{1}{2} R(z) I^2(z) + \frac{1}{2} G(z) V^2(z) \right] dz \quad (1)$$

where l is horizontal span of the line, $I(z)$ and $V(z)$ are position-dependent current and voltage amplitudes of the standing wave mode, and $R(z)$ and $G(z)$ are the series resistance and shunt conductance per unit length at z . In order to obtain the minimum-loss tapered line, we should find $R(z)$ and $G(z)$ that minimize P_{diss} above under the constraint of the R - G tradeoff. However, it is very difficult to evaluate the integration above since $I(z)$ and $V(z)$ are not known *a priori*, as they depend on the line structure, which has yet to be determined.

To appreciate the difficulty in evaluating (1), imagine the following scenario. We start with a uniform line, in which $I(z)$ and $V(z)$ are sinusoids. We then find $R(z)$ and $G(z)$ that minimize (1) for these sinusoidal amplitude variations. These $R(z)$ and $G(z)$ are z -dependent, thus corresponding to a tapered line structure, upon which $I(z)$ and $V(z)$ are no longer sinusoids. However, the $R(z)$ and $G(z)$ were based on the sinusoidal amplitude variations, and hence, this tapered line is not optimized for the new non-sinusoidal amplitude profiles. Thus an iteration process is required, making the optimization procedure involved.

Fortunately, evaluation of (1) is substantially simplified by our novel transformation [1] in which the integration variable, z , of (1) is mapped to θ , the wave's phase. When a wave travels down on a general tapered line, its infinitesimal phase change is given by $d\theta = [\omega/v(z)] \cdot dz$ at position z assuming a weak loss, where ω is the modal frequency and $v(z)$ is the wave velocity. Since by design the characteristic impedance is held at a constant value Z_0 , there is no local reflection and the wave's phase at z is the simple accumulation of the infinitesimal phase change:

$$\theta(z) = \omega \int_0^z \sqrt{L(z')C(z')} dz' \quad (2)$$

where we have used $v(z) = 1/\sqrt{L(z)C(z)}$ [$L(z)$ and $C(z)$ are inductance and capacitance per unit length at z].

This transformation from z to $\theta(z)$ is powerful because the voltage and current amplitudes for a standing wave mode are *always* sinusoids of the phase, $\theta(z)$, *regardless* of the specific shape of the tapered line of the constant characteristic impedance:

$$V(z) = V_0 \cos \theta(z), \quad I(z) = I_0 \sin \theta(z) \quad (3)$$

where V_0 is the voltage maximum, I_0 is the current maximum, and $Z_0 = V_0/I_0$. Note from (2) and (3) that the voltage and current amplitudes are very complicated functions of z , reflecting the difficulty of the integration in the z domain. Now with the transformation of the integration variable from z to θ using (2), (1) is greatly simplified to:

$$P_{diss} = \int_0^{\pi/2} \left[\frac{1}{2}(I_0 \sin \theta)^2 R_\theta(\theta) + \frac{1}{2}(V_0 \cos \theta)^2 G_\theta(\theta) \right] d\theta \quad (4)$$

where we have assumed that the line length is chosen as to produce $\pi/2$ total phase shift ($\lambda/4$ SWO). Here $R_\theta(\theta) \equiv R(z) \cdot (dz/d\theta)$ and $G_\theta(\theta) \equiv G(z) \cdot (dz/d\theta)$ are series and shunt loss per radian phase shift where $dz/d\theta$ is obtained from (2). Now one can easily obtain the minimum-loss tapered line in the θ -domain, by finding $R_\theta(\theta)$ and $G_\theta(\theta)$ that minimize P_{diss} in (4). Evaluating (4) is easy since the current and voltage standing waveforms are always known sinusoids in the θ -domain regardless of the line shape.

The constraint for the minimization of P_{diss} is the previously mentioned R - G tradeoff. Using $R_\theta G_\theta = \text{const.}$ as a hypothetical constraint,² minimization of (4) becomes an elementary mathematical exercise [1]: one can easily obtain both the minimum-loss tapered line and the minimum-loss uniform line with their corresponding power dissipations, comparison between which reveals that the loss in the minimum-loss tapered line is smaller by a factor of $2/\pi$ than that in the minimum-loss uniform line [1]. This loss comparison assumed that both of the transmission lines of the same characteristic impedance, Z_0 , host the same (in the θ -domain) standing waves (at an identical modal frequency, ω) given by (3), and hence this comparison is meaningful only when the standing waves store the same amount of energy in both transmission lines. This is indeed the case as seen in the following.

When hosting the standing waves given by (3), any general $\lambda/4$ tapered transmission line with constant characteristic impedance Z_0 stores a total time-averaged energy given by

$$E_{stored} = \int_0^{\pi/2} \left[\frac{1}{4}(I_0 \sin \theta)^2 L_\theta(\theta) + \frac{1}{4}(V_0 \cos \theta)^2 C_\theta(\theta) \right] d\theta \quad (5)$$

where $L_\theta(\theta) \equiv L(z) \cdot (dz/d\theta)$ and $C_\theta(\theta) \equiv C(z) \cdot (dz/d\theta)$ are inductance and capacitance per radian phase shift. Using (2) and $\sqrt{L(z)/C(z)} = Z_0$, we find $L_\theta(\theta) = Z_0/\omega$ and $C_\theta(\theta) = 1/(\omega Z_0)$, which are independent of θ but solely determined by ω and Z_0 . Since the minimum-loss tapered line and the minimum-loss uniform line above have the same Z_0 and ω , they also have the same L_θ and C_θ . This, in conjunction with (5), means that the tapered and uniform optimum lines store exactly the same amount of energy. Hence the loss reduction calculation above is meaningful since it was performed when the minimum-loss tapered and uniform lines store the same amount of energy. Moreover, the loss reduction by a factor of $\pi/2$ due to tapering translates directly to a $\pi/2$ improvement in Q . The analysis above

²This reflects the real-world situation quite well [1].

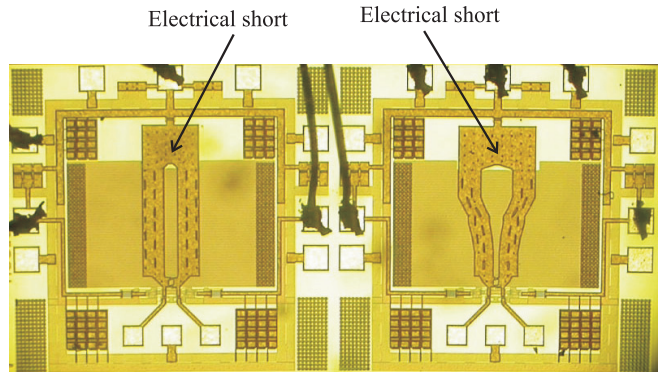


Fig. 4. MOS SWO with uniform (left) and tapered (right) CPS.

conveys a quantitative idea on Q enhancement owing to the tapering. The real-world improvement due to tapering is closed to this theoretical prediction (see below).

C. Wave Adaptive Line Tapering - Design

The findings from the preceding analysis are crucial in the practical design of the tapered line. As is the key to the analysis, evaluation of the power dissipation in a tapered line is much easier in the θ -domain than in the z -domain. Therefore the minimum-loss tapered line is first designed in the θ -domain. To this end, a comprehensive set of EM-simulated data that are R_θ , G_θ , C_θ , and L_θ values for a wide range of w and s values (various uniform lines) are to be first prepared. Using the data, one can perform a piecewise construction of the minimum-loss tapered line by putting segments of the various uniform lines of the same characteristic impedance together in such a way that local loss in every θ -position is minimized.³ Equation (4) is useful in evaluating the loss to determine the optimal apportionment of the various uniform line configurations. After this θ -domain construction, one can translate the design into the z -domain using (2) to create the physical layout. Detailed design procedure can be found in [1].

Figure 4 shows the die photo of the SWOs with the minimum-loss uniform and tapered CPS from [1], which were implemented in a $0.18\mu\text{m}$ CMOS technology. The uniform CPS SWO was implemented for the comparison purposes. The uniform CPS has a simulated Q of 39 at 15 GHz⁴, and the tapered CPS hosting the standing wave has a higher effective Q of $39 \times 1.5 \approx 59$, a considerable number for an on-chip resonator in silicon. The improvement factor of 1.5 is close to the previous theoretical prediction of $\pi/2$. Figure 5 shows the measured phase noise for both the tapered-CPS and uniform-CPS SWOs (both SWOs oscillated around 15 GHz). The phase noise improvement as large as 10 dB due to the increased Q from the tapering is evident, attesting to the validity of the wave-adaptive line tapering concept.

D. Wave Adaptive Line Tapering - "Wave Control" Perspective -

During optimization of the tapered line, it is most convenient to think of the line primarily in terms of its circuit

³A finite number of uniform lines mimic a continuous tapered line.

⁴This high Q is due to floating metals placed under the CPS [1].

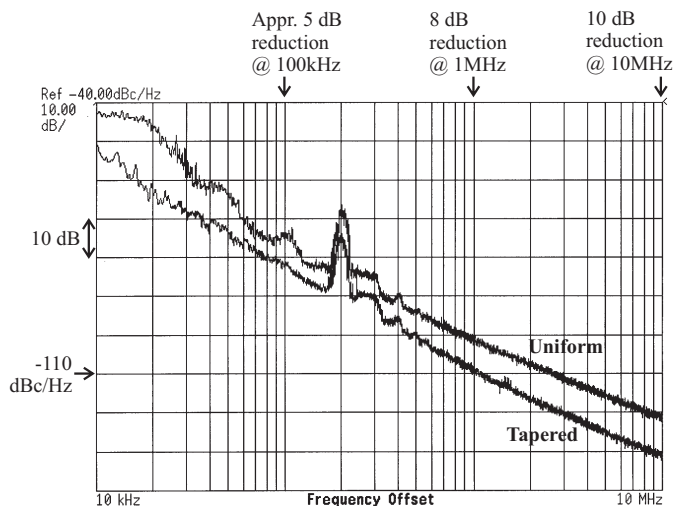


Fig. 5. Measured phase noise for the tapered- & uniform-CPS SWOs.

model and its component values, and to view tapering simply as a modification of the circuit as we exclusively did in the preceding subsections. This perspective, however, can obscure the view of tapering as a modification of the field distributions which comprise the EM standing wave. By altering w and s , we are actually controlling the 3D spatial shapes of the wave's fields. Let us consider a transverse cross section of the transmission line. The thin and closely spaced metals at $z = 0$ in Fig. 3(b) correspond to areally confined, relatively dense electric and magnetic fields; the wider, spaced metals at $z = l$ in Fig. 3(b) correspond to more voluminous, diffuse fields. Thus the wave becomes more dispersed at positions closer to $z = l$.

This alternate perspective permits a physical understanding of why loss mechanisms are reduced after tapering. The electric field is stronger than the magnetic field at $z = 0$ due to the voltage maximum and current minimum. Losses associated with the electric field occur due to the interactions with the underlying substrate, so one would expect that by utilizing a tight configuration (small w & s), the electric field will concentrate close to the metals rather than permeating the substrate and thus yield minimal loss. Indeed, this intuition matches our findings from the circuit model. Similarly, toward the electrical short there is a magnetic field maximum and electric field minimum. Moving the metals apart disperses the magnetic field, reducing the electron-bunching force and thus dissipation in the metals. Thus tapering can be thought of as controlling the wave's physical shape to avoid lossy interactions.

III. ELECTRICAL SOLITON OSCILLATOR

Now we turn to the second subject of this paper, a review of the electrical soliton oscillator that we recently reported in [2] (See also [12] & [13]). This circuit that self-generates a periodic train of nonlinear pulse-shape waves known as electrical solitons is a noticeable departure from the conventional sinusoidal wave-based oscillator type. We shall first introduce solitons to provide background in the following subsection; the subsequent subsections will review the main subject, the electrical soliton oscillator.

A. Solitons - Primer

Solitons are a unique class of pulse-shaped waves that propagate in nonlinear dispersive media. They maintain spatial confinement of energy in a pulse shape in propagation and exhibit singular nonlinear dynamics. Balance between nonlinearity and dispersion creates the soliton phenomena. Common in nature, solitons are found in various nonlinear dispersive media, *e.g.*, water, plasma, solid-state crystals, and optical fibers.

In the electrical domain, the nonlinear transmission line (NLTL), a 1D ladder network of inductors and varactors [Fig. 1(a)] or alternatively a linear transmission line periodically loaded with varactors [Fig. 6(a)], serves as a nonlinear dispersive wave propagation medium [10]. The nonlinearity originates from the varactors while the dispersion arises from the structural periodicity. For certain pulse-shaped voltage waves, the nonlinearity balances out the dispersion, and they propagate on the NLTL maintaining their exact shape (in the absence of loss). These are electrical solitons. The general soliton propagation solution on the NLTL is a periodic train of solitons [Fig. 6(b)]. In the presence of loss, the solitons cannot maintain their exact shape in the course of propagation, but they still maintain spatial confinement of wave energy in a pulse shape through a unique damping process [14].

In addition to their ability to maintain spatial confinement of wave energy, the electrical solitons on the NLTL possess other unique properties. To begin with, a taller soliton travels faster than a shorter one. Due to this amplitude-dependent speed, if a taller soliton is placed behind a shorter one as shown in Fig. 6(c) top, the taller one will catch up with the shorter one and move ahead of it after a collision [Fig. 6(c)]. When two solitons collide [middle of Fig. 6(c)], they do *not* linearly superpose and experience significant amplitude modulations (nonlinear collision). After the collision [bottom of Fig. 6(c)], the two solitons have returned to their original shapes, but have acquired a permanent time (phase) shift, shown by the difference in d_1 and d_2 in Fig. 6(c). The three soliton properties above, *i.e.*, 1) *amplitude-dependent speed*, 2) *amplitude modulation during the collision*, and 3) *phase modulation after the collision*, unless well-controlled, will become obstacles in constructing the soliton oscillator, leading to oscillation instabilities as will be seen in the next section.

Non-soliton waves can also travel on the NLTL, but only by changing their shape to form into a soliton or solitons. A non-soliton pulse close to soliton shape will be sharpened into a soliton [Fig. 6(d), top]. A non-soliton pulse that is significantly different from soliton shape will break up into multiple solitons of different amplitudes [Fig. 6(d), bottom]. It is these transient soliton-forming processes that have been widely exploited in the traditional 2-port NLTL approach [Fig. 1(a)] to generate sharp electrical pulses [10].

B. Electrical Soliton Oscillator - Operating Principles "Control of the Unruly Soliton Waves"

As pointed out in Sec. I, the essence of our work [2] is the construction of an oscillator that *self-generates* a pe-

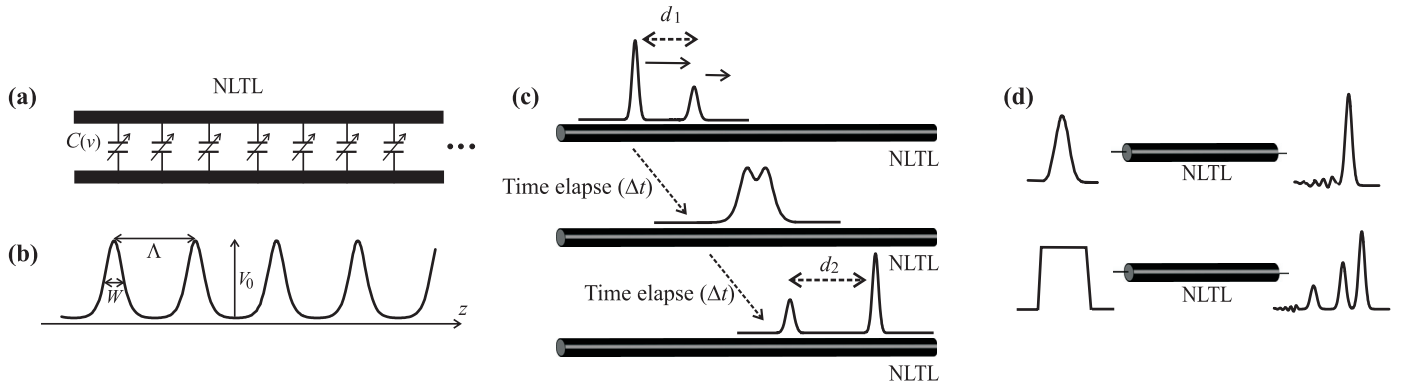


Fig. 6. (a) NLTL: a linear transmission line periodically loaded with varactors. (b) A general soliton waveform. (c) Depiction of electrical solitons' amplitude-dependent speed and nonlinear collision. $d_1 \neq d_2$. (d) Hypothetical transient, soliton-forming processes on the NLTL.

riodic train of electrical solitons without requiring an external high-frequency input. Almost all the previous electrical soliton work used the NLTL as a 2-port system that requires an external high-frequency input to generate the soliton output. The distinction of our approach from the traditional approach is captured in Fig. 1.

The starting idea to build our soliton oscillator was to combine a ring NLTL with a non-inverting amplifier inserted in the ring [Fig. 7(a)]. The ring NLTL supports certain soliton circulation modes determined by the periodic boundary condition, $l = n\Lambda$ ($n = 1, 2, 3, \dots$) (l : ring circumference, Λ : spacing between two adjacent solitons) [Fig. 7(b)]. The amplifier is intended to provide gain to initiate a startup and to compensate loss in steady state. The ultimate goal of this topology is to self-generate and self-sustain one of the soliton circulation modes of Fig. 7(b).

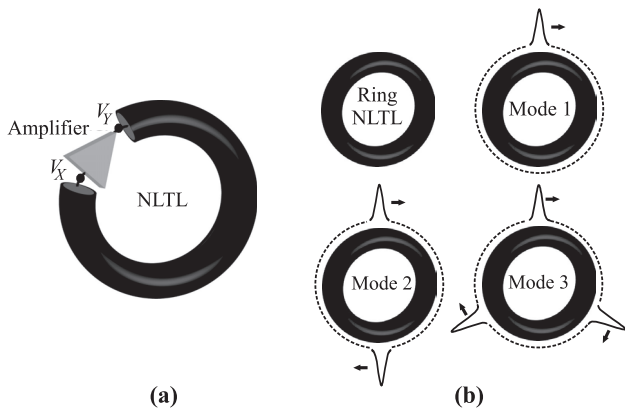


Fig. 7. (a) Soliton oscillator topology. (b) Ring NLTL and Modes.

The topology does indeed lead to oscillations, self-starting from noise. However, when standard amplifiers are used in the topology, the oscillations tend to be plagued with instability problems, exhibiting significant variations in pulse amplitude and repetition rate [2], [11] [Fig. 8]. The oscillation instabilities arise because the circular loop topology of Fig. 7(a) not only generates the desired soliton circulation mode, but can also excite other parasitic solitons [2]. The desired and parasitic solitons continually collide while circulating in the loop due to their generally different amplitudes and resultant speed difference (due to solitons' amplitude-dependent speed, Subsec. III-

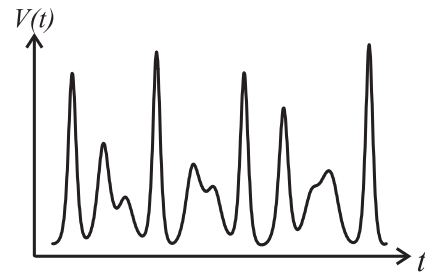


Fig. 8. Unstable oscillations that can result from Fig. 7(a).

A). These soliton collision events cause the modulations in the pulse amplitude and repetition rate (Subsec. III-A), leading to the oscillation instabilities.

The key to our success in building a stable electrical soliton oscillator in [2] is to develop a special amplifier in Fig. 7(a), which not only provides gain but also incorporates three stability mechanisms to prevent the soliton collision events in steady state. The stability mechanisms are:

(1) *Reduced signal saturation*: If the amplifier saturates its output significantly in Fig. 7(a), the amplifier output will be close to a square pulse. As explained with Fig. 6(d), bottom, this square pulse will break apart into multiple solitons of differing amplitudes propagating down the NLTL. These multiple solitons will circulate around the loop at different speeds (due to the amplitude-dependent speed), and be again distorted by the amplifier, creating even more solitons of different amplitudes and speeds. This process repeats itself, and the solitons continue to circulate in the loop at different speeds, continually colliding with one another, causing oscillation instabilities. It is therefore necessary to minimize distortion.

(2) *Perturbation rejection*: In steady-state oscillation the amplifier should attenuate any small ambient perturbation (e.g., noise) that could otherwise grow into parasitic solitons. Unless this is achieved, the desired soliton circulation mode and parasitic solitons will propagate at different speeds due to their generally different amplitudes, colliding and building up oscillation instabilities.

(3) *Single mode selection*: The amplifier should select a single soliton circulation mode in steady-state oscillation among the many possible modes [Fig. 7(b)]. If this is not achieved, various modes with generally different amplitudes will circulate in the loop at different speeds, leading to

soliton collision events and hence unstable oscillations.

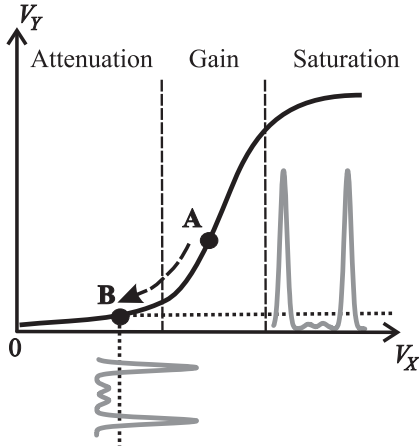


Fig. 9. Transfer curve of a saturating amplifier. Startup bias **A** is in the gain region. As the dc component of the amplifier output increases in initial transient, the bias is adaptively lowered (dashed arrow) towards steady-state bias **B**.

In [2], we achieved these stability mechanisms in an amplifier by incorporating an adaptive bias control in a standard saturating amplifier. Figure 9, showing the input-output transfer curve of the saturating amplifier, explains how this is achieved. The transfer curve is divided into the attenuation, gain, and saturation regions based on the curve's tangential slopes. At startup the amplifier is biased at point **A** in the gain region so that ambient noise can be amplified to initiate the oscillation startup. As the oscillation grows and forms into a pulse train, the dc component of the amplifier output increases. This increase in the dc component is used to adaptively lower the amplifier bias (dashed arrow in Fig. 9). The reduced bias corresponds to an overall gain reduction, since a portion of the pulse enters the attenuation region. The bias point continues to move down on the curve until the overall gain becomes equal to the system loss, settling at the steady-state bias **B**.

In steady state with the bias at **B**, the three stability mechanisms are simultaneously satisfied. First, the reduced bias ensures that the peak portions of the input pulses do not enter the saturation region, reducing distortion (*reduced signal saturation*). Second, with the reduced bias, the steady-state input soliton train is placed *across* the attenuation and gain regions, causing small perturbations around the bias to be attenuated (*perturbation rejection*). Note that perturbation rejection is accomplished while maintaining gain for the main portions of the input soliton train to compensate loss. This threshold-dependent gain-attenuation mechanism is a technique widely employed in modelocked lasers in optics, where it is known as *saturable absorption*. Third, the dependence of the steady-state bias on the dc component of the output leads to a mode-dependant gain since each mode has a different dc component. This naturally allows for the selection of one particular mode (*single mode selection*).

The amplifier with the adaptive bias scheme could be implemented in various ways: an example is in Fig. 10. The amplifier consists of two inverting stages: one built around an nMOS transistor, M_1 , and the other built around a

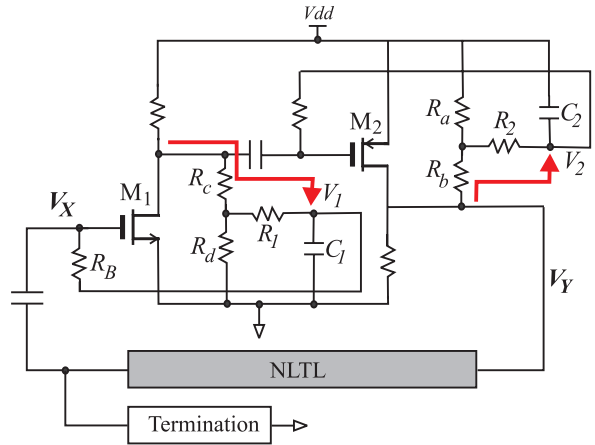


Fig. 10. Example stabilizing amplifier schematic.

pMOS transistor, M_2 . The adaptive bias scheme is implemented for both stages. It works as follows for the pMOS stage. The output waveform, V_Y , is sensed by the voltage divider consisting of R_a and R_b , and then is integrated by the R_2 - C_2 network. The integrated voltage V_2 represents a scaled dc component of V_Y . This dc component is fed back to the gate of M_2 to set its bias. As the dc level of V_Y increases, V_2 will increase, reducing the gate-source voltage of M_2 , effectively lowering its bias. A similar argument goes for the nMOS stage. Combining, the input bias of the amplifier decreases as the dc component of V_Y increases, performing the adaptive bias control.

C. Electrical Soliton Oscillator - Experiments

We have developed three soliton oscillator prototypes that have confirmed the circuit concepts. The first two prototypes [2] were built using discrete components (measured pulse widths: 43 ns and 827 ps) to explicitly examine the detailed dynamics of the oscillator. The third prototype [12] was implemented on a CMOS integrated circuit (measured pulse width: 293 ps). Figure 11 shows the measured steady-state soliton oscillations from each prototype.

The most fascinating dynamics of the soliton oscillator can be observed by following the pulse around the oscillator loop in steady state. Figure 12 shows such spatial dynamics measured from our first prototype [2]. At the output of the amplifier the pulse (width: 100 ns) is not exactly a soliton and, hence, sharpens into a soliton while propagating down the NLTL. Once the soliton is formed at the eighth section (width: 43 ns), it does not further sharpen since it is now a soliton. Instead, the loss on the NLTL becomes the dominant process, and the soliton exhibits soliton damping [14] as it further travels down the NLTL, reducing its amplitude and velocity while increasing its width. At the end of the NLTL, the pulse width has increased to 110 ns. It is this clear existence of the transition point between the two distinctive processes, the pulse sharpening and widening, that unequivocally confirms the formation of the soliton at that transition point.

D. Future Extensions and Applications

The minimum pulse width of 293 ps achieved in our latest prototype [12] is not a record number as compared to the

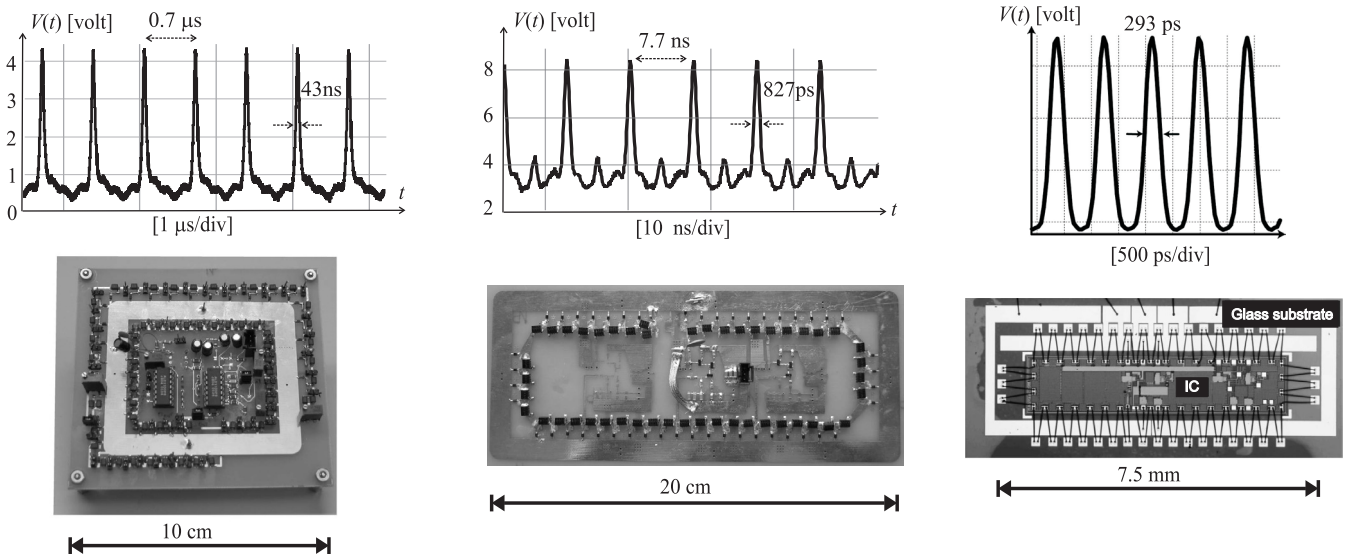


Fig. 11. (Left) First soliton oscillator (pulse width: 43 ns, pulse repetition rate: 1.4 MHz). (Center) Second soliton oscillator (width: 827 ps, repetition: 130 MHz). (Right) Third, chip-scale soliton oscillator (width: 293 ps, repetition: 1.14 GHz)

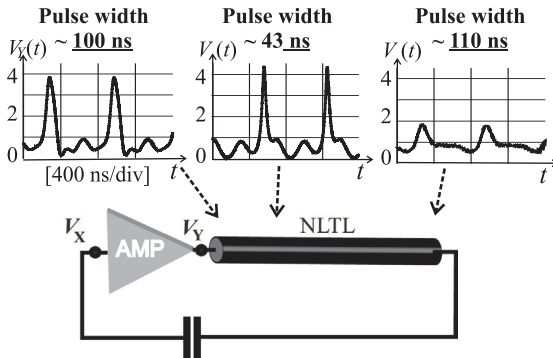


Fig. 12. Measured spatial dynamics of the first soliton oscillator [2].

state-of-the-art 2-port NLTL (480 fs rise time) [15]. The value of our work so far, rather, lies in the demonstration of the soliton oscillator concept: the ability to self-generate stable solitons. Now with the concept firmly demonstrated, it can be quickly scaled to a much higher speed. For example, the ultrafast NLTL in [15] can be incorporated in our soliton oscillator to substantially reduce the soliton width.

Placing such an ultrafast NLTL in the soliton oscillator raises an important question on the impact of the amplifier bandwidth on the minimum soliton width. While the propagation of a 1-ps wide pulse on the stand-alone NLTL is feasible [15], amplifiers, even in the state-of-the-art solid-state technologies, cannot provide bandwidth for such a sharp pulse. The experimental results in Fig. 12 clearly suggest, however, that the soliton compression on the NLTL may be able to overcome the bandwidth limitation of the amplifier, and hence, it may be feasible to achieve a 1-ps pulse width using the NLTL of [15] despite the relatively slower amplifier. The explicit demonstration of this interesting possibility remains an open question, and would be a natural future extension of this work.

Such picosecond electrical soliton oscillators will offer a new platform for all-electrical ultrafast time-domain metrology. This is because the short pulse duration directly translates to high temporal resolution in time-domain mea-

surements. The narrow electrical pulses can be used to sample, or take “snapshots” of, rapidly varying electrical signals with picosecond temporal resolution [10], which is currently possible only with expensive lasers. Similarly, the picosecond electrical pulses can be used as probe signals for high-precision time-domain reflectometry (TDR) [16].

IV. ACKNOWLEDGEMENT

We thank M. DePetro of Harvard, T. H. Lee of Stanford, and L. DeVito & R. Sullivan of ADI for support. D. Ham thanks AFOSR, ETRI, IBM, NSF, and NIH.

REFERENCES

- [1] W. Andreas and D. Ham, “Standing wave oscillators utilizing wave-adaptive tapered transmission lines,” *IEEE JSSC*, vol. 40, no. 3, pp. 638-651, March 2005.
- [2] D. S. Ricketts, X. Li, and D. Ham, “Electrical soliton oscillator,” *IEEE T-MTT*, vol. 54, no. 1, pp. 373-382, Jan. 2006
- [3] R. H. Varian and S. F. Varian, “A high frequency oscillator and amplifier,” *J. Appl. Phys.*, vol. 10, pp. 321-327, May 1939.
- [4] L. Divina *et al.*, “The distributed oscillator at 4 GHz,” *IEEE T-MTT*, vol. 46, no. 12, pp. 2240 - 2243, Dec. 1998.
- [5] B. Kleveland *et al.*, “Monolithic CMOS distributed amp. and osc.,” *IEEE ISSCC*, pp. 70-71, Feb. 1999.
- [6] H. Wu *et al.*, “Silicon-based distributed voltage-controlled oscillators,” *IEEE JSSC*, vol. 36, no. 3, Mar. 2001.
- [7] J. Wood *et al.*, “Rotary travelling-wave oscillator arrays: a new clock technology,” *IEEE JSSC*, vol. 36, no. 11, Nov. 2001.
- [8] F. O’Mahony *et al.*, “10GHz clock distribution using coupled SWOs,” *IEEE ISSCC*, pp. 428-429, Feb. 2003.
- [9] D. Ham and W. Andreas, “A circular standing wave oscillator,” *IEEE ISSCC*, pp. 380-381, 2004.
- [10] M. J. Rodwell *et al.*, “Active and nonlinear wave propagation devices in ultrafast electronics and optoelectronics,” *Proc. IEEE*, vol. 82, no. 7, pp. 1037-1059, July 1994.
- [11] G. J. Ballantyne, *Periodically Amplified Soliton Systems*, PhD Dissertation, University of Canterbury, New Zealand, 1994.
- [12] D. S. Ricketts and D. Ham, “A chip-scale electrical soliton oscillator,” *IEEE ISSCC*, pp. 432-433, Feb. 2006.
- [13] T. H. Lee, “Electrical solitons come of age,” *Nature* vol. 440, pp. 36-37, March 2006.
- [14] E. Ott and R. N. Sudan, “Damping of solitary waves,” *The Physics of Fluids*, vol. 13, no. 6, pp. 1432-1434, June 1970.
- [15] D. van der Weide, *APL*, vol. 65, pp. 881-883, August 1994.
- [16] B. Elliot, “High-sensitivity picosecond time-domain reflectometry,” *IEEE Trans. Instrum. Meas.*, vol. IM-25, Dec. 1976.